Geometric atom interferometry with shortcuts to adiabaticity

Yan-Xiong Du,[1] Xian-Xian Yue,[1] Zhen-Tao Liang,[1] Jia-Zhen Li,[1] Hui Yan,[1,*] and Shi-Liang Zhu[1,2,3,†]

[1]*Guangdong Provincial Key Laboratory of Quantum Engineering and Quantum Materials, SPTE, South China Normal University, Guangzhou 510006, China*

[2]*National Laboratory of Solid State Microstructures, School of Physics, Nanjing University, Nanjing 210093, China*

[3]*Synergetic Innovation Center of Quantum Information and Quantum Physics, University of Science and Technology of China, Hefei 230026, China*

(Received 12 December 2016; published 6 April 2017)

Realization of the highly efficient π and $\pi/2$ pulses is crucial in an atom interferometry. Here we propose a scheme to realize these operations based on an intrinsically fault-tolerant geometric phase and stimulated Raman shortcuts to the adiabatic passage. The scheme is fast due to the shortcuts to adiabaticity and is robust based on the geometric phase. In the presence of various noises, we show that the fringe contrast of the proposed interferometer is higher than that of the resonant Raman pulse and the stimulated Raman adiabatic passage. Furthermore, the scheme is demonstrated to be especially suitable for applications that require a large space-time area enclosed by interfering wave packets.

DOI: 10.1103/PhysRevA.95.043608

I. INTRODUCTION

Light-pulse atom interferometry, a hallmark tool of precision measurements, plays a critical role in the test of inertial forces [1–5] and fundamental physical constants [6–9]. Furthermore, highly sensitive light-pulse atom interferometry has been proven to be a promising technology for inertial navigators [10–12]. The critical ingredients of light-pulse atom interferometry are the $\pi/2$ and π light pulses, which split or recombine the atomic wave packets [13]. Realization of such operations with high quality is thus fundamentally important in atom interferometry. Two-photon stimulated Raman transition is the traditional way to coherently realize such pulses [14,15].

Several significant technologies have been developed to improve the quality of these light pulses, all with limitations. Since the sensitivity of the atom interferometer scales linearly with the space-time area enclosed by the interfering wave packets [16–18], sequential application of stimulated Raman transitions can be used to increase the momentum transfer [19]. However, the interference fringe contrast of an atom interferometer is sensitive to system errors, such as the velocity distribution of the cold atoms and the inhomogeneous intensity distribution of the laser field [20,21]. An alternative way to improve the quality of interferometry is stimulated Raman adiabatic passage (STIRAP), which has been demonstrated to be a robust way to achieve the π and $\pi/2$ pulses [22–24]. However, the losing of atoms from the third excited state significantly decreases the interference fringe contrast a lot. Very recently, the frequency-swept Raman adiabatic passage has proven to be a highly efficient and robust way to split the atomic wave packets [21,25]. However, in order to maintain the adiabatic condition, Raman adiabatic passage requires a long evolution time, which will limit the increase of large momentum transfer. Therefore, further development of π and $\pi/2$ light pulses with fast and robust features is of significant importance in achieving atom interferometry.

In this paper, we propose a light-pulse atom interferometry based on an intrinsically fault-tolerant geometric phase and stimulated Raman shortcut to adiabatic passage (STIRSAP). The π and $\pi/2$ operations can be realized with a nontrivial dynamic phase or a pure geometric phase. The latter has been shown to be robust against certain errors [26]. For instance, geometric quantum gates [27] have recently been experimentally realized in various quantum computing candidates [28–30], and they have been demonstrated to be of the highest fidelity in the nitrogen-vacancy centers [29]. Furthermore, it has been experimentally demonstrated in a superconducting qubit that the contrast of the Landau-Zener interferometry with a pure geometric phase is higher than that of the counterpart based on a nontrivial dynamic phase [31]. On the other hand, the applications of the adiabatic protocols are limited by the requirement of slow driving, which conflicts with the feebleness of quantum coherence when the system of interest is embedded in an environment. Shortcuts to adiabaticity protocols can solve this difficulty [32–36]. We demonstrate that our scheme combines the advantages of the geometric operations and the advantages of shortcuts to adiabaticity, especially in the multipulse experiments: the employment of shortcuts to adiabatic passages makes the manipulation faster than Raman adiabatic passages and more robust than stimulated Raman transition; the $\pi/2$ and π operations are realized through geometric phases and are thus protected by the geometric characteristic and resilient to random errors. The scheme is easy to realize in experiments, requiring only the modulation of the Raman pulse shapes. Fast and robust to systemic and random errors, our protocol is especially suitable for atomic interferometry applications that require a the large momentum transfer.

The paper is organized as follows: Section II introduces the dressed states and the realization of $\pi/2$ and π pulses without dynamical phase by adiabatic passages. Section III shows how to accelerate the adiabatic manipulations by reshaping the pulse shapes. In Sec. IV we discuss the measurement characteristics of the interferometers. In Sec. V, we use the geometric operation to realize multi-π atom interferometer. We conclude this paper in Sec. VI.

*yanhui@scnu.edu.cn
†slzhu@nju.edu.cn

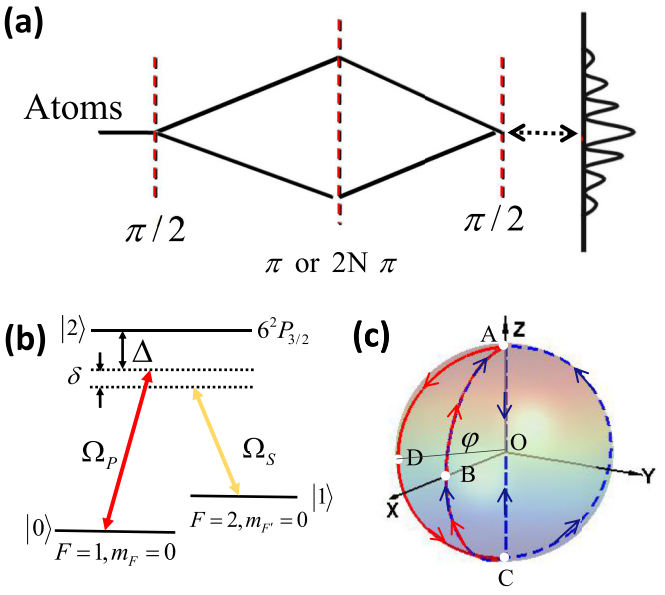

FIG. 1. (a) A Mach-Zehnder atom interferometer composed of the $\pi/2-\pi-\pi/2$ pulses. The middle π pulse can be replaced with multi-π pulses to increase the momentum transfer. (b) The laser-atom coupling scheme. Ω_P: pumping laser; Ω_S: Stoke laser; Δ: single-photon detuning; δ: two-photon detuning. (c) Evolution paths of cyclic state (red solid line) on the Bloch sphere to realize geometric $\pi/2$ and π operations. Cyclic state initialized in state $|\lambda_+\rangle$ will evolve along the path B-A-D-C-B and pick up a geometric phase. The blue dashed line depicts the trace of effective magnetic field in the parameter space.

II. GEOMETRIC PHASE AND ADIABATIC MANIPULATION

We consider a Mach-Zehnder atom interferometer as shown in Fig. 1(a). The interferometer is composed of a $\pi/2$ pulse that divides the atom wave packet, a π pulse that brings the wave packets back together, and a second $\pi/2$ pulse that overlaps the wave packets to create interference [13]. To obtain a larger momentum transfer, one can replace the middle π pulse with $2N$ pulses (N being an integer). The $\pi/2$-π-$\pi/2$ pulses can be realized with various approaches. For atom interferometry with two-photon stimulated Raman transition, these light pulses can be realized by Rabi oscillation with large single detuning and two photon resonant, which is fast but not robust against the system errors (i.e., variation in Rabi frequencies or detuning). For atom interferometry with STIRAP, the light pulses can be realized by ordinary STIRAP with simultaneous single- and two- photon resonance, which is robust against the system errors, but nevertheless is sensitive to the spontaneous emission from the excited state. For atom interferometry with frequency-swept Raman adiabatic passage, the light pulses can be realized through sweeping the two-photon detuning with large single-photon detuning, which is also robust; however, both STIRAP and the frequency-swept Raman adiabatic passage are not fast because the adiabatic condition requires the evolution to be sufficiently slow. Different from the above three approaches, we propose to realize the geometric $\pi/2$ and π light pulses through a shortcut to adiabatic passage with large single detuning and two-photon resonant.

As shown in Fig. 1(b), we consider the ^{133}Cs atoms and the energy levels chosen as $|0\rangle = |6S_{1/2}, F = 1, m_F = 0\rangle$, $|1\rangle = |6S_{1/2}, F = 2, m_{F'} = 0\rangle$, and $|2\rangle = |6P_{3/2}\rangle$ [37]. The states $|0\rangle, |2\rangle, |1\rangle$ are coupled by the pumping and Stokes laser fields with Rabi frequencies Ω_P and Ω_S, respectively. Using the rotating-wave approximation, the system Hamiltonian under the interaction picture is $H_0^I(t) = \hbar/2(\Omega_P e^{i\varphi}|0\rangle\langle 2| + \Omega_S|1\rangle\langle 2| + 2\Delta|2\rangle\langle 2| + 2\delta|1\rangle\langle 1| + \text{H.c.})$, where Δ is the single-photon detuning, δ is the two-photon detuning, and φ is the relative phase between pumping and Stokes lasers. For $\Delta \gg \Omega_{P,S}$, the excited state $|2\rangle$ can be adiabatically eliminated and the Hamiltonian $H_0^I(t)$ can be reduced to an effective two-level system based on $|0\rangle$, $|1\rangle$:

$$H_{\text{eff}}(t) = \frac{\hbar}{2}\begin{pmatrix} -\Delta_{\text{eff}} & \Omega_{\text{eff}} e^{-i\varphi} \\ \Omega_{\text{eff}} e^{i\varphi} & \Delta_{\text{eff}} \end{pmatrix}, \tag{1}$$

where $\Delta_{\text{eff}} = [\Omega_P^2(t) - \Omega_S^2(t)]/4\Delta$ and $\Omega_{\text{eff}} = -\Omega_P(t)\Omega_S(t)/2\Delta$. The system will evolve in the subspace spanned by the two lower dressed states $\{|\lambda_-\rangle, |\lambda_+\rangle\}$, where $|\lambda_-\rangle = \cos\theta|0\rangle - \sin\theta e^{-i\varphi}|1\rangle$, and $|\lambda_+\rangle = \sin\theta e^{i\varphi}|0\rangle + \cos\theta|1\rangle$, with $\delta = 0$ and $\theta(t) = \arctan\frac{\Omega_P(t)}{\Omega_S(t)}$.

In the adiabatic case, the eigenstates $|\lambda_-\rangle$, $|\lambda_+\rangle$ become cyclic states under the driving of control parameters. For the system prepared in an initial state $|\psi_i\rangle$, it can be expanded as $|\psi_i\rangle = a_+|0\rangle + a_-|1\rangle = a_+|\lambda_+(0)\rangle + a_-|\lambda_-(0)\rangle$. After a cyclical evolution with adiabatic manipulation, the final state will be $|\psi_f\rangle = a_+e^{i\gamma}|\lambda_+(T)\rangle + a_-e^{-i\gamma}|\lambda_-(T)\rangle = a_+e^{i\gamma}|\lambda_+(0)\rangle + a_-e^{-i\gamma}|\lambda_-(0)\rangle$. Here γ is the geometric phase, and the dynamical phase is ignored since it can be canceled by the spin-echo method described later. The final state and the initial state can be linked by an evolution operator $U_{(\chi,\gamma)}$, which is derived as

$$U_{(\chi,\gamma)} = \begin{pmatrix} \cos\gamma + i\sin\gamma\cos\chi & i\sin\chi\sin\gamma \\ i\sin\chi\sin\gamma & \cos\gamma - i\sin\gamma\cos\chi \end{pmatrix}, \tag{2}$$

where $\chi = \theta(0)$ [38,39]. When choosing $\chi = \pi/2$ and $\gamma = \pi/4$, the evolution operator becomes

$$U_{(\pi/2,\pi/4)} = \frac{\sqrt{2}}{2}\begin{pmatrix} 1 & i \\ i & 1 \end{pmatrix},$$

which is $\pi/2$ pulse; when choosing $\chi = \pi/2$ and $\gamma = \pi/2$, the evolution operator with the form

$$U_{(\pi/2,\pi/2)} = i\begin{pmatrix} 0 & 1 \\ 1 & 0 \end{pmatrix}$$

is π pulse operation.

In the following, we describe in detail how to realize the above geometric operations by adiabatic passages [40,41]. The general expression of the pumping pulses and Stokes pulses in STIRAP are given by

$$\Omega_P(t) = \Omega_0 \exp\left(\frac{-t^2}{b^2}\right)\sin\beta + \Omega_0 \exp\left(\frac{-(t+\tau)^2}{b^2}\right)\sin\alpha,$$
$$\Omega_S(t) = \Omega_0 \exp\left(\frac{-t^2}{b^2}\right)\cos\beta + \Omega_0 \exp\left(\frac{-(t+\tau)^2}{b^2}\right)\cos\alpha, \tag{3}$$

where Ω_0 is the peak value of Rabi frequency, τ is the delay time between the laser pulses, and b is the full width at half maximum of pulses. The parameter $\theta(t)$ can be adjusted by the value of α and β. When $t \to -\infty, \theta(-\infty) = \alpha$; when $t \to \infty$, $\theta(\infty) = \beta$. To achieve geometric phases, one should drive the cyclic states (namely, the eigenstates $|\lambda_-\rangle$, $|\lambda_+\rangle$) evolving along the closed path on the Bloch sphere. By parametrizing the state vector with $\langle\psi|\sigma_i|\psi\rangle$ (σ_i is the Pauli matrices), $i = x, y, z$, the cyclic state initialized in $|\lambda_+\rangle$ will evolve along the path B-A-D-C-B in our scheme as shown by the red curve in Fig. 1(c). The variation of θ corresponding to the curve B-A-D-C-B is given by $\frac{\pi}{4} \to 0 \to \frac{\pi}{4} \to \frac{\pi}{2} \to \frac{\pi}{4}$. By changing the relative phase φ, we can change the value of geometric phase. The $\pi/2$ pulse can be realized when $\varphi = \pi/4$, while the π pulse is achieved when $\varphi = \pi/2$.

A concern with using adiabatic passage is the accumulation of the dynamical phases, which can be canceled by the spin-echo method. The Hamiltonian (1) can be rewritten as $H_{\rm eff}(t) = -(\hbar/2)\sigma \cdot \mathbf{B}$, where σ is the Pauli matrices $\{\sigma_x, \sigma_y, \sigma_z\}$ and $\mathbf{B} = (\Omega_{\rm eff}\sin\varphi, \Omega_{\rm eff}\cos\varphi, \Delta_{\rm eff})$ is the effective magnetic field. We remove the dynamical phases by reversing the field $\mathbf{B}$ [$\Delta_{\rm eff}(t) \to -\Delta_{\rm eff}(T-t)$, $\varphi(t) \to \varphi(T-t)+\pi$] at the half time of the evolution, which results in $H_{\rm eff}(t) = -H_{\rm eff}(T-t)$ [39]. The trace of the effective magnetic field $\mathbf{B}$ is shown in Fig. 1(c) by the blue dashed line. The modification of $\Delta_{\rm eff}$ can be realized by controlling $\theta(t)$, while a π phase should be added at point C to invert φ.

III. ACCELERATION BY SHORTCUTS TO ADIABATIC PASSAGE

We now address a shortcut method to accelerate adiabatic passage [32–36,42,43]. As the adiabatic evolution requires the adiabatic condition, the evolution is usually time consuming. According to the theory of shortcuts to adiabaticity [32,33], we can suppress the diabatic transition and speed up the procedure by adding an auxiliary Hamiltonian given by

$$H_{\rm cd}(t) = \frac{\hbar}{2}\begin{pmatrix} 0 & -i\Omega_{\rm a}(t)e^{i\varphi_{\rm a}} \\ i\Omega_{\rm a}(t)e^{-i\varphi_{\rm a}} & 0 \end{pmatrix}, \qquad (4)$$

where $\Omega_{\rm a}(t) = 2(\Omega_{\rm P}\dot{\Omega}_{\rm S} - \dot{\Omega}_{\rm P}\Omega_{\rm S})/(\Omega_{\rm P}^2 + \Omega_{\rm S}^2)$ and $\varphi_{\rm a} = \varphi - \pi/2$. By choosing a suitable unitary transformation [33,34] that does not change state at the initial and final times, one can further incorporate the contribution of $H_{\rm cd}$ into the pulse shapes. Therefore, by using the modified pulse shapes given by [35]

$$\tilde{\Omega}_{\rm P}(t) = \sqrt{2\Delta\left(\sqrt{\tilde{\Delta}_{\rm eff}^2(t) + \tilde{\Omega}_{\rm eff}^2(t)} + \tilde{\Delta}_{\rm eff}(t)\right)},$$
$$\tilde{\Omega}_{\rm S}(t) = \sqrt{2\Delta\left(\sqrt{\tilde{\Delta}_{\rm eff}^2(t) + \tilde{\Omega}_{\rm eff}^2(t)} - \tilde{\Delta}_{\rm eff}(t)\right)}, \qquad (5)$$

where $\tilde{\Delta}_{\rm eff}(t) = \Delta_{\rm eff} + \dot{\phi}, \tilde{\Omega}_{\rm eff}(t) = \sqrt{\Omega_{\rm eff}^2 + \Omega_{\rm a}^2}$, and $\phi = \arctan(\Omega_{\rm a}/\Omega_{\rm eff})$ are the modified effective detuning and Rabi frequency, we can realize fast transfer along adiabatic passage by only adjusting the pulses shapes [44].

Here we compare the population dynamics of π pulses as driven by STIRAP and STIRSAP. We choose the system parameters as $\Omega_0 = 2\pi \times 4$ MHz, $\Delta = 2\pi \times 0.5$ GHz,

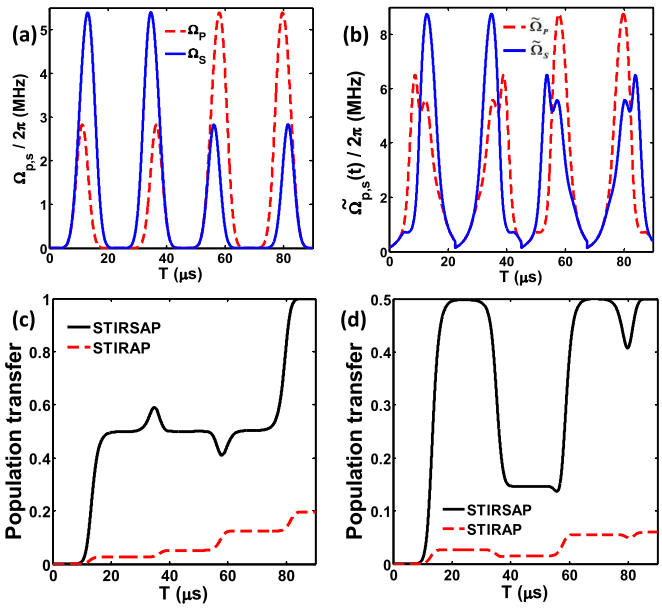

FIG. 2. (a) The pulse shapes $\Omega_{\rm P}(t)$ and $\Omega_{\rm S}(t)$ for the geometric π pulse according to Eq. (3). (b) The pulse shapes of $\tilde{\Omega}_{\rm P}(t)$ and $\tilde{\Omega}_{\rm S}(t)$ for the modified π pulse according to Eq. (5). The population dynamics of geometric π pulses (c) and $\pi/2$ pulses (d) driven by the STIRSAP (black solid line) and STIRAP (red dashed line), respectively. Note that the adiabatic is not fulfilled here; STIRAP cannot realize perfect transfer. However, STIRSAP can realize perfect transfer after eliminating the diabatic effect.

$T_{\rm s} = 22.5\ \mu$s, $b = T_{\rm s}/8$, and $\tau = -T_{\rm s}/8$, where $T_{\rm s}$ is the operation time of single fractional STIRAP, and the total operation time is $T = 4T_{\rm s} = 90\ \mu$s. The pulse shapes of $\Omega_{\rm P}$ and $\Omega_{\rm S}$ are plotted in Fig. 2(a), which drive the quantum states evolving along the closed path by STIRAP. According to Eq. (5), the modified pulse shapes of STIRSAP are plotted in Fig. 2(b). The initial state of the system is set to be $|0\rangle$. We plot the population transferred to $|1\rangle$ as driven by STIRAP and STIRSAP in Fig. 2(c). The final population of STIRAP is less than 20% since the adiabatic condition is not satisfied [$(\Omega_0^2/2\Delta)T \approx 2.88\pi$]. However, after we suppress the diabatic effect by modifying the pulse shapes, the final population of STIRSAP can reach 100% with the same operation time T. Similar results are obtained for the $\pi/2$ pulse as shown in Fig. 2(d). The population transfer of an ideal $\pi/2$ pulse should be 50%; however it is less than 10% when the STIRAP is used without the adiabatic condition, while the population transfer of STIRSAP reaches the expected value of 50% with the same operation time.

IV. RANDOM NOISE AND SYSTEMIC ERROR

It has been shown that geometric quantum gates in quantum computation are insensitive to fast varying random fluctuations [38,45,46]. Similarly, here we demonstrate that, since our method is intrinsically geometric, it is also insensitive to certain random fluctuations with relatively high frequencies. In Fig. 3(a), we plot the transfer efficiencies of π pulses under three kinds of interferometers (resonant Raman pulses, STIRAP, and STIRSAP) versus the amplitude of random

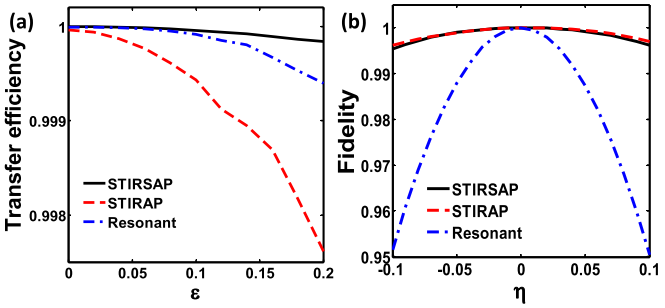

FIG. 3. (a) The π pulse transfer efficiency for the STIRSAP (black solid line), STIRAP (red dashed line), and resonant Raman pulses (blue dashed-dotted line) vs the amplitude of random fluctuation. The plots are averaged over 500 times. (b) The fidelity of interferometers for the same parameters in (a) vs the deviation of Rabi frequency. The operation times of the resonant Raman pulses (blue dashed-dotted line), STIRAP (red dashed line), and STIRSAP (black solid line) are 13 μs, 2.7 ms, and 0.27 ms, respectively.

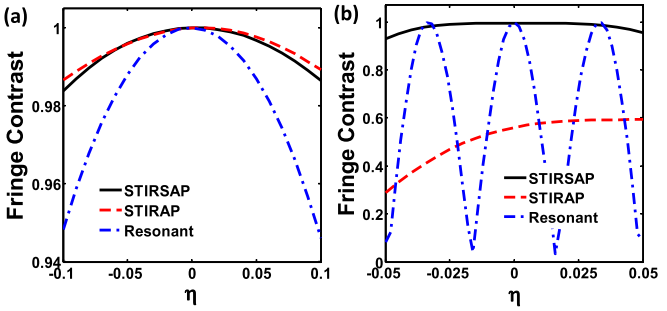

FIG. 4. The fringe contrasts of the $\pi/2$-π-$\pi/2$ interferometers (a) and the interferometers with 30 intermediate π pulses (b) for the STIRSAP (black solid line), STIRAP (red dashed line), and resonant Raman pulses (blue dashed-dotted line) vs the deviation of Rabi frequency.

fluctuation in Rabi frequency. The randomized fluctuation is artificially introduced by adding an amplitude shift to Ω_0. The actual Rabi frequency is written as $\Omega' = (1+\varepsilon)\Omega_0$, where ε has 1000 points of noise and a mean value of zero. The transfer efficiency of π pulse driven by STIRSAP is almost stable at 1 when ε increases up to 20%, while the transfer efficiencies for both resonant Raman pulses and STIRAP are lower. Thus the simulation reveals STIRSAP is more robust than resonant Raman pulses and STIRAP at a noise frequency higher than 10 kHz.

A major systemic error in an atom interferometer is the amplitude shift of Rabi frequency, which comes mainly from the inhomogeneous distribution of the laser fields and the velocity distribution of the cold atoms [47]. We compare three different ways to realize the $\pi/2$-π-$\pi/2$ atom interferometer (resonant Raman pulses, STIRAP, and STIRSAP), where the maximum Rabi frequencies of the three methods are the same. The system parameters are chosen to be the same with the ones in Fig. 2(a). The operation times of the resonant Raman, STIRAP, and STIRSAP are $T_{\mathrm{R}} = 13\ \mu$s, $T_{\mathrm{A}} = 2.7$ ms, and, $T_{\mathrm{SA}} = 0.27$ ms, respectively. We plot in Fig. 3(b) the fidelity of the final states as a function of the variation of Rabi frequency. The fidelity is defined as $F = \sqrt{\mathrm{Tr}(\rho_{\mathrm{ideal}} \cdot \rho)}$, where Tr denotes the trace of the matrix, ρ is the actual density matrix, and ρ_{ideal} is the ideal density matrix of the final state [48]. The variation of Rabi frequency is set to be $\Omega' = (1+\eta)\Omega_0$, $\eta \in [-0.1, 0.1]$. The fidelity of interferometer driven by resonant Raman pulses drops to 95% when the Rabi frequency deviates from Ω_0 by 10%, as shown in Fig. 3(b). However, the fidelity of interferometers driven by STIRAP and STIRSAP are higher than 99.5% with the same deviation, with STIRSAP needing only one-tenth of the operation time of STIRAP.

It should be noted that there is also imperfection in two-photon detuning, which is introduced by the Zeeman shift and the unwanted ac Stark light shift. The Zeeman shift can be suppressed by choosing magnetic-insensitive levels $m_{\mathrm{F}} = 0$ as ground states. The unwanted ac Stark shift comes from the virtual coupling, namely, Ω_{P} couples $|1\rangle \longleftrightarrow |2\rangle$ and Ω_{S} couples $|0\rangle \longleftrightarrow |2\rangle$. The ac Stark shift of virtual coupling can be calculated as $\delta_{ac} = \frac{|\Omega_P|^2}{4\Delta_{P,12}} + \frac{|\Omega_S|^2}{4\Delta_{S,02}}$, where $\Delta_{P,12}$, $\Delta_{S,02}$ is the detuning between the coupling laser and the coupled energy level. With atom ^{133}Cs (the ground states' splitting is about 9 GHz) and suitable single-photon detuning $\Delta = 2\pi \times 0.5$ GHz, δ_{ac} induced by the virtual coupling is smaller than $2\pi \times$ 50 Hz. The ac Stark shift has been taken into account in the calculation of transfer, nevertheless, it has little influence on the results.

We next compare the fringe contrasts of the interferometers versus the variation of Rabi frequency. By tilting the relative phase of the last $\pi/2$ pulse, we will get a fringe where the final population of $|1\rangle$ changes with the relative phase. The fringe contrast of the interferometer is defined as $V = (P_{\max} - P_{\min})/(P_{\max} + P_{\min})$, where $P_{\max}$ is the maximum of the population and $P_{\min}$ is the minimum of the population. As shown in Fig. 4(a), the fringe contrast of the interferometer composed of resonant Raman pulses drops to 95% when Rabi frequency deviates from Ω_0 by 10%. In contrast, the fidelity composed by STIRAP and STIRSAP are higher than 98.5%. Therefore, the interferometer based on STIRSAP is more robust than resonant Raman pulses against control parameter variations, and it needs much less operation time than the adiabatic passages.

V. MULTI-π-PULSE ATOM INTERFEROMETER

The robustness of the geometric atom interferometer with STIRSAP implies that our proposal can be generalized to multi-π-pulse cases, which can be used to realize large momentum transfer [16–18]. Here we consider an atom interferometer with 30 intermediate π pulses. We compare the multi-π-pulse interferometers realized by resonant Raman pulses, STIRAP, and STIRSAP; the total evolution times are 0.20 ms, 28.8 ms (with adiabatic condition satisfied), and 2.88 ms, respectively. Since the typical ground-state coherence time of cold atoms is about $T_c = 40$ ms [49], we take into account the decoherence when simulating the evolutions. The decoherence effect can be introduced by revising the final population P by an exponential decay factor of $P(T) = (1 + \exp -T^2/T_c^2)/2|P_{\mathrm{id}}(T)|^2$ [50], where T is the period and P_{id} is the population without decoherence. The fringe contrast as a function of the Rabi frequency shift is shown in Fig. 4(b).

The resonant Raman pulses reveal an oscillation behavior when the Rabi frequency changes. The contrast of resonant Raman pulses is high at a certain point; however, it drops quickly due to the average effect among the atomic ensemble. Though the operation time of STIRAP is long enough to satisfy the adiabatic condition, its fringe contrast is not high due to the decoherence effect. A high fringe contrast is achieved when we choose STIRSAP to realize the atom interferometer because the operation is robust and the operation time is short and avoids the decoherence effect. Therefore, STIRSAP is a promising way to realize a large momentum transfer in the atom interferometers.

VI. CONCLUSIONS

In summary, we have proposed a useful scheme of atom interferometry based on a geometric phase and shortcuts to adiabatic passages. The scheme is easy to realize in experiments and combines STIRSAP's fast feature and the geometric operation's resilience towards the random fluctuation. Therefore, the proposed fast and robust atom interferometer may pave a way to precision measurements. For example, the detailed applications of the present scheme to a kind of special atom interferometry, such as the interferometries used to test inertial forces and fundamental physical constants or for inertial navigators, deserve further exploring.

ACKNOWLEDGMENTS

This work was supported by the NKRDP of China (Grants No. 2016YFA0301803 and No. 2016YFA0302800), the NSF of China (Grants No. 11474107 and No. 91636218), the GDSBPYSTIT (Grant No. 2015TQ01X715), the GNSFDYS (Grant No. 2014A030306012), the FOYTHEG (Grant No. Yq2013050), the PRNPGZ (Grant No. 2014010), the NSF of Guangdong province (Grant No. 2016A030310462), and SRFYTSCNU (15KJ15).

Y.X.D. and X.X.Y. contributed equally to this work.

[1] A. Peters, K. Y. Chung, and S. Chu, Measurement of gravitational acceleration by dropping atoms, Nature (London) **400**, 849 (1999).

[2] A. Peters, K. Y. Chung, and S. Chu, High-precision gravity measurements using atom interferometry, Metrologia **38**, 25 (2001).

[3] T. L. Gustavson, A. Landragin, and M. A. Kasevich, Rotation sensing with a dual atom-interferometer Sagnac gyroscope, Class. Quantum Grav. **17**, 2385 (2000).

[4] L. Zhou, S. T. Long, B. Tang, X. Chen, F. Gao, W. C. Peng, W. T. Duan, Z. Q. Zhang, Z. Y. Zong, J. Wang, Y. Z. Zhang, and M. S. Zhan, Test of Equivalence Principle at 10^{-8} Level by a Dual-Species Double-Diffraction Raman Atom Interferometer, Phys. Rev. Lett. **115**, 013004 (2015).

[5] X. C. Duan, X. B. Deng, M. K. Zhou, K. Zhang, W. J. Xu, F. Xiong, Y. Y. Xu, C. G. Shao, J. Luo, and Z. K. Hu, Test of the Universality of Free Fall with Atoms in Different Spin Orientations, Phys. Rev. Lett. **117**, 023001 (2016).

[6] P. Clade, E. D. Mirandes, M. Cadoret, S. G. Khelifa, C. Schwob, F. Nez, L. Julien, and F. Biraben, Determination of the Fine Structure Constant Based on Bloch Oscillations of Ultracold Atoms in a Vertical Optical Lattice, Phys. Rev. Lett. **96**, 033001 (2006).

[7] J. B. Fixler, G. T. Foster, J. M. McGuirk, and M. A. Kasevich, Atom interferometer measurement of the Newtonian constant of gravity, Science **315**, 74 (2007).

[8] G. Lamporesi, A. Bertoldi, L. Cacciapuoti, M. Prevedelli, and G. M. Tino, Determination of the Newtonian Gravitational Constant Using Atom Interferometry, Phys. Rev. Lett. **100**, 050801 (2008).

[9] S. W. Chiow, S. Herrmann, S. Chu, and H. Muller, Noise-Immune Conjugate Large-Area Atom Interferometers, Phys. Rev. Lett. **103**, 050402 (2009).

[10] B. Canuel, F. Leduc, D. Holleville, A. Gauguet, C. J. Borde, A. Landragin, and P. Bouyer, Six-Axis Inertial Sensor Using Cold-Atom Interferometry, Phys. Rev. Lett. **97**, 010402 (2006).

[11] R. Geiger, V. Menoret, G. Stern, N. Zahzam, P. Cheinet, F. Moron, A. Bresson, A. Landragin, and P. Bouyer, Detecting inertial effects with airborne matter-wave interferometry, Nat. Commun. **2**, 474 (2011).

[12] A. V. Rakholia, H. J. McGuinness, and G. W. Biedermann, Dual-Axis High-Data-Rate Atom Interferometer via Cold Ensemble Exchange, Phys. Rev. Appl. **2**, 054012 (2014).

[13] A. D. Cronin, J. Schmiedmayer, and D. E. Pritchard, Optics and interferometry with atoms and molecules, Rev. Mod. Phys. **81**, 1051 (2009).

[14] M. Kasevich and S. Chu, Atomic Interferometry Using Stimulated Raman Transitions, Phys. Rev. Lett. **67**, 181 (1991).

[15] T. L. Gustavson, P. Bouyer, and M. A. Kasevich, Precision Rotation Measurements with an Atom Interferometer Gyroscope, Phys. Rev. Lett. **78**, 2046 (1997).

[16] D. L. Butts, K. Kotru, J. M. Kinast, A. M. Radojevic, B. P. Timmons, and R. E. Stoner, Efficient broadband Raman pulses for large-area atom interferometry, J. Opt. Soc. Am. B **30**, 922 (2013).

[17] H. Muller, S. W. Chiow, Q. Long, S. Herrmann, and S. Chu, Atom Interferometry with up to 24-Photon-Momentum-Transfer Beam Splitters, Phys. Rev. Lett. **100**, 180405 (2008).

[18] S. W. Chiow, T. Kovachy, H. C. Chien, and M. A. Kasevich, 102$\hbar$k Large Area Atom Interferometers, Phys. Rev. Lett. **107**, 130403 (2011).

[19] J. M. McGuirk, M. J. Snadden, and M. A. Kasevich, Large Area Light-Pulse Atom Interferometry, Phys. Rev. Lett. **85**, 4498 (2000).

[20] J. Martin, B. W. Shore, and K. Bergmann, Coherent population transfer in multilevel systems with magnetic sublevels. II. Algebraic analysis, Phys. Rev. A **52**, 583 (1995).

[21] K. Kotru, J. M. Brown, D. L. Butts, J. M. Kinast, and E. Stoner, Robust Ramsey sequences with Raman adiabatic rapid passage, Phys. Rev. A **90**, 053611 (2014).

[22] P. Marte, P. Zoller, and J. L. Hall, Coherent atomic mirrors and beam splitters by adiabatic passage in multilevel systems, Phys. Rev. A **44**, R4118(R) (1991).

[23] M. Weitz, B. C. Young, and S. Chu, Atomic Interferometer Based on Adiabatic Population Transfer, Phys. Rev. Lett. **73**, 2563 (1994).

[24] L. S. Goldner, C. Gerz, J. C. Spreeuw, S. L. Rolston, C. I. Westbrook, W. D. Phillips, P. Marte, and P. Zoller, Momentum Transfer in Laser-Cooled Cesium by Adiabatic Passage in a Light Field, Phys. Rev. Lett. **72**, 997 (1994).

[25] K. Kotru, D. L. Butts, J. M. Kinast, and E. Stoner, Large-Area Atom Interferometry with Frequency-Swept Raman Adiabatic Passage, Phys. Rev. Lett. **115**, 103001 (2015).

[26] G. D. Chiara and G. M. Palma, Berry Phase for a Spin 1/2 Particle in a Classical Fluctuating Field, Phys. Rev. Lett. **91**, 090404 (2003).

[27] P. Zanardi and M. Rasetti, Holonomic quantum computation, Phys. Lett. A **264**, 94 (1999).

[28] D. Leibfried, B. DeMarco, V. Meyer, D. Lucas, M. Barrett, J. Britton, W. M. Itano, B. Jelenkovic, C. Langer, T. Rosenband, and D. J. Wineland, Experimental demonstration of a robust, high-fidelity geometric two ion-qubit phase gate, Nature (London) **422**, 412 (2003).

[29] C. Zu, W. B. Wang, L. He, W. G. Zhang, C. Y. Dai, F. Wang, and L. M. Duan, Experimental realization of universal geometric quantum gates with solid-state spins, Nature (London) **514**, 72 (2014).

[30] A. A. Abdumalikov, J. M. Fink, K. Juliusson, M. Pechal, S. Berger, A. Wallraff, and S. Filipp, Experimental realization of non-Abelian non-adiabatic geometric gates, Nature (London) **496**, 482 (2013); G. Feng, G. Xu, and G. Long, Experimental Realization of Nonadiabatic Holonomic Quantum Computation, Phys. Rev. Lett. **110**, 190501 (2013).

[31] X. Tan, D. W. Zhang, Z. Zhang, Y. Yu, S. Han, and S. L. Zhu, Demonstration of Geometric Landau-Zener Interferometry in a Superconducting Qubit, Phys. Rev. Lett. **112**, 027001 (2014).

[32] M. V. Berry, Transitionless quantum driving, J. Phys. A: Math. Theor. **42**, 365303 (2009).

[33] X. Chen, I. Lizuain, A. Ruschhaupt, D. Guery-Odelin, and J. G. Muga, Shortcut to Adiabatic Passage in Two-and Three-Level Atoms, Phys. Rev. Lett. **105**, 123003 (2010).

[34] M. G. Bason, M. Viteau, N. Malossi, P. Huillery, E. Arimondo, D. Ciampini, R. Fazio, V. Giovannetti, R. Mannella, and O. Morsch, High-fidelity quantum driving, Nat. Phys. **8**, 147 (2012).

[35] Y. X. Du, Z. T. Liang, Y. C. Li, X. X. Yue, Q. X. Lv, W. Huang, X. Chen, H. Yan, and S. L. Zhu, Experimental realization of stimulated Raman superadiabatic passage with cold atoms, Nat. Commun. **7**, 12479 (2016).

[36] S. An, D. Lv, A. del Campo, and K. Kim, Shortcuts to adiabaticity by counterdiabatic driving for trapped-ion displacement in phase space, Nat. Commun. **7**, 12999 (2016).

[37] R. Stoner, D. Butts, J. Kinast, and B. Timmons, Analytical framework for dynamic light pulse atom interferometry at short interrogation times, J. Opt. Soc. Am. B **28**, 2418 (2011).

[38] Z. T. Liang, X. X. Yue, Q. X. Lv, Y. X. Du, W. Huang, H. Yan, and S. L. Zhu, Proposal for implementing universal superadiabatic geometric quantum gates in nitrogen-vacancy centers, Phys. Rev. A **93**, 040305(R) (2016).

[39] S. L. Zhu and Z. D. Wang, Implementation of Universal Quantum Gates Based on Nonadiabatic Geometric Phases, Phys. Rev. Lett. **89**, 097902 (2002); Universal quantum gates based on a pair of orthogonal cyclic states: Application to NMR systems, Phys. Rev. A **67**, 022319 (2003).

[40] J. Bateman and T. Freegarde, Fractional adiabatic passage in two-level systems: Mirrors and beam splitters for atomic interferometry, Phys. Rev. A **76**, 013416 (2007)

[41] C. M. Simon, T. Belhadj, B. Chatel, T. Amand, P. Renucci, A. Lemaitre, O. Krebs, P. A. Dalgarno, R. J. Warburton, X. Marie, and B. Urbaszek, Robust Quantum dot Exciton Generation Via Adiabatic Passage with Frequency-Swept Optical Pulses, Phys. Rev. Lett. **106**, 166801 (2011).

[42] M. Demirplak and S. A. Rice, Adiabatic population transfer with control fields, J. Phys. Chem. A **107**, 9937 (2003).

[43] M. Demirplak and S. A. Rice, Assisted adiabatic passage revisited, J. Phys. Chem. B **109**, 6838 (2005).

[44] The spin-echo method in the adiabatic manipulation to remove dynamical phases can be generalized to the shortcut to adiabatic passage, because the auxiliary Hamiltonian $H_{\rm cd}(t)$ will not contribute dynamical phases ($\langle n|H_{\rm cd}|n\rangle = i\hbar\Sigma_n(\langle n|\partial_t n\rangle\langle n|n\rangle) = 0$ with $n = \lambda_\pm$).

[45] S.-L. Zhu and P. Zanardi, Geometric quantum gates that are robust against stochastic control errors, Phys. Rev. A **72**, 020301(R) (2005).

[46] P. Solinas, P. Zanardi, and N. Zanghi, Robustness of non-Abelian holonomic quantum gates against parametric noise, Phys. Rev. A **70**, 042316 (2004).

[47] A. Hilico, C. Solaro, M. K. Zhou, M. Lopez, and F. P. D. Santos, Contrast decay in a trapped-atom interferometer, Phys. Rev. A **91**, 053616 (2015).

[48] X. Zhang, R. P. d. Aguila, T. Mazzoni, N. Poli, and G. M. Tino, Trapped-atom interferometer with ultracold Sr atoms, Phys. Rev. A **94**, 043608 (2016).

[49] I. Buluta, S. Ashhab, and F. Nori, Natural and artificial atoms for quantum computation, Rep. Prog. Phys. **74**, 104401 (2011).

[50] A. Daniel, R. Agou, O. Amit, D. Groswasser, Y. Japha, and R. Folman, Damping of local Rabi oscillations in the presence of thermal motion, Phys. Rev. A **87**, 063402 (2013).